doi:10.1038/nature11729

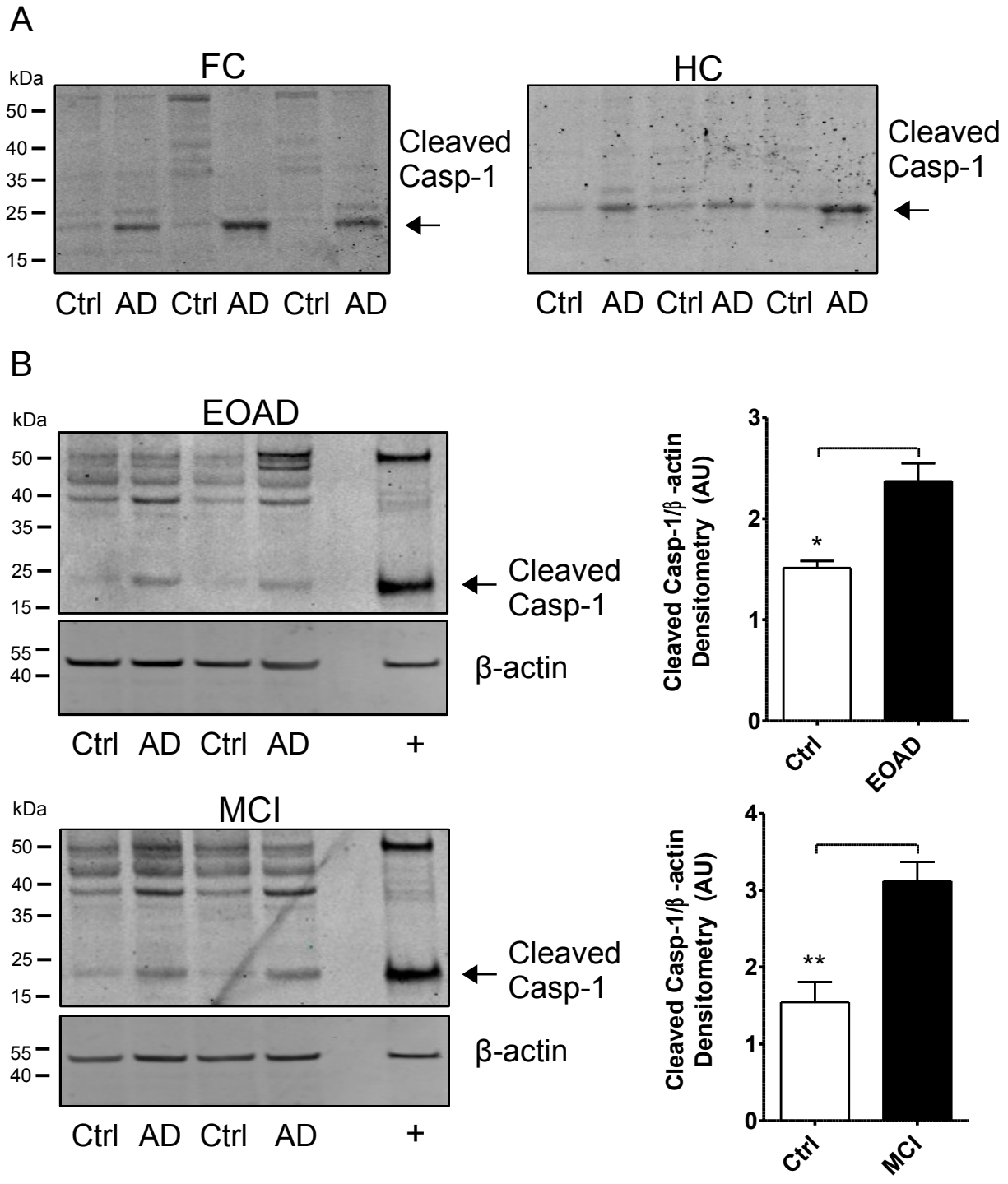

Suppl. Figure 1. Detection of cleaved caspase-1 (Casp-1) in human brain samples. (A) Brain samples from frontal cortex (FC) and hippocampal (HC) samples from Alzheimer patients (AD) and controls (Ctrl), shown in Fig.1 A, here detected by a caspase-1 antibody (gift from Dr. Gabriel Nuñez). **(B)** Analysis of early onset AD cases (EOAD) and mild cognitive impairment (MCI) patients frontal cortex brain samples obtained from the Banner Health collection. β-actin served as loading control. Quantitation by densitometric analysis (mean of n=3 for control and n=12 for EOAD/MCI ±SEM; Student´s t-test, * $p<0.05$, ** $p<0.01$).

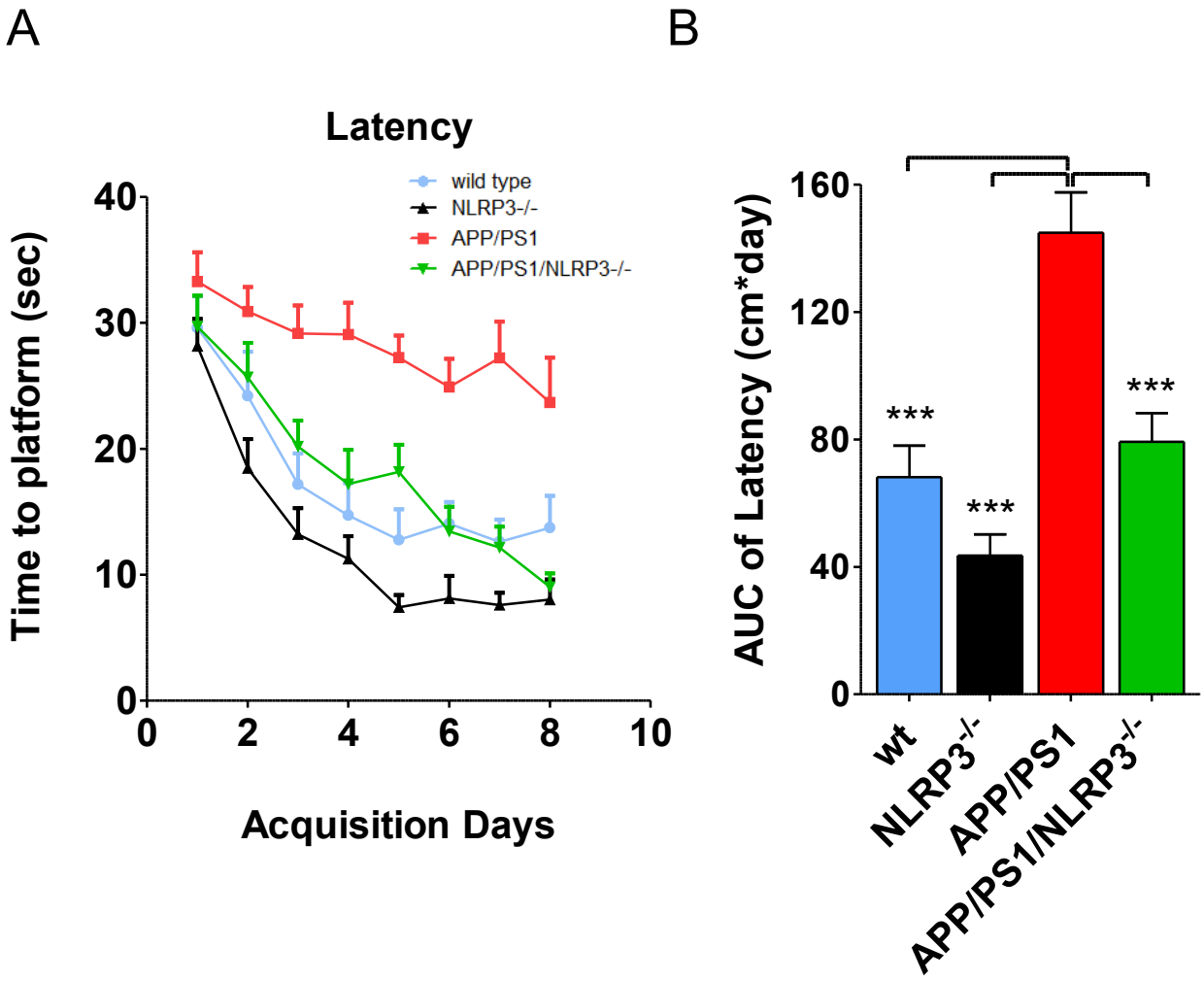

Suppl. Figure 2. NLRP3 gene deficiency protects APP/PS1 transgenic mice from spatial memory deficits at 16 months of age. Spatial memory was assessed by Morris water maze testing. **(A)** Time needed to reach the hidden platform (latency) in wild-type (wt), NLRP3$^{-/-}$, APP/PS1, and APP/PS1/NLRP3$^{-/-}$ mice. **(B)** Integrated time travelled (AUC = area under the curve) (mean of n=16 for wt, n=12 for NRLP3$^{-/-}$, n=14 for APP/PS1, and n=15 for APP/PS1/NLRP3$^{-/-}$ ±SEM; one-way ANOVA, Tukey´s post hoc test, *** $p<0.001$).

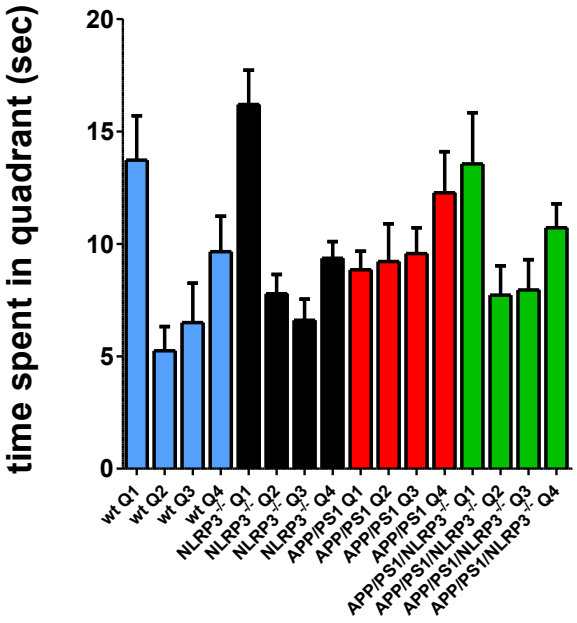

Suppl. Figure 3. Morris water maze - probe trial. At day 9, 24 h after the last training session, a spatial probe trial were conducted, where the platform was removed and the time animals spent in the quadrants was recorded. Probe trial data given as time spent in quadrant (sec) for each genotype and quadrant. Q1 represents the quadrant in which the platform had been located from day 1-8. Wt, NLRP3$^{-/-}$ and APP/PS1/NLRP3$^{-/-}$ showed a clear preference for the target quadrant Q1, whereas APP/PS1 mice did not spend more time in the target quadrant than in the other quadrants.

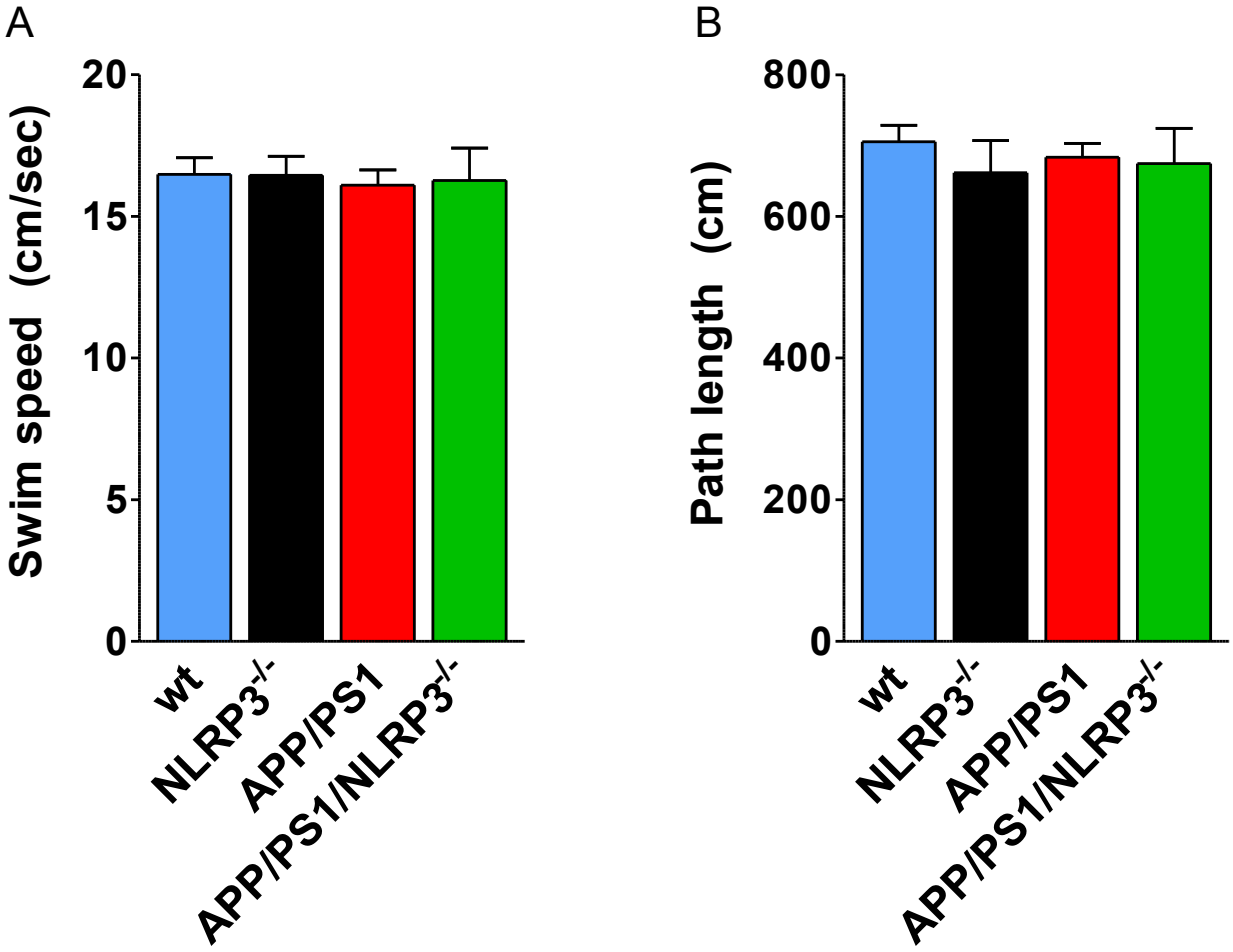

Suppl. Figure 4. Morris water maze - swim speed and path length. To exclude differences in motor performance between animals, **(A)** swim speed (cm/sec) and **(B)** path length (cm) during the Morris Water Maze test were recorded and analyzed by the video tracking software Ethovision 3.1 (Noldus, Wageningen, The Netherlands). Mean swim speed (v) was calculated by the equation v=distance/time and is given as cm/sec. Statistical analysis did not reveal any significant differences between groups (mean of n=16 for wt, n=12 for NRLP3$^{-/-}$, n=14 for APP/PS1, and n=15 for APP/PS1/NLRP3$^{-/-}$ ±SEM; one-way ANOVA, Tukey´s post hoc test).

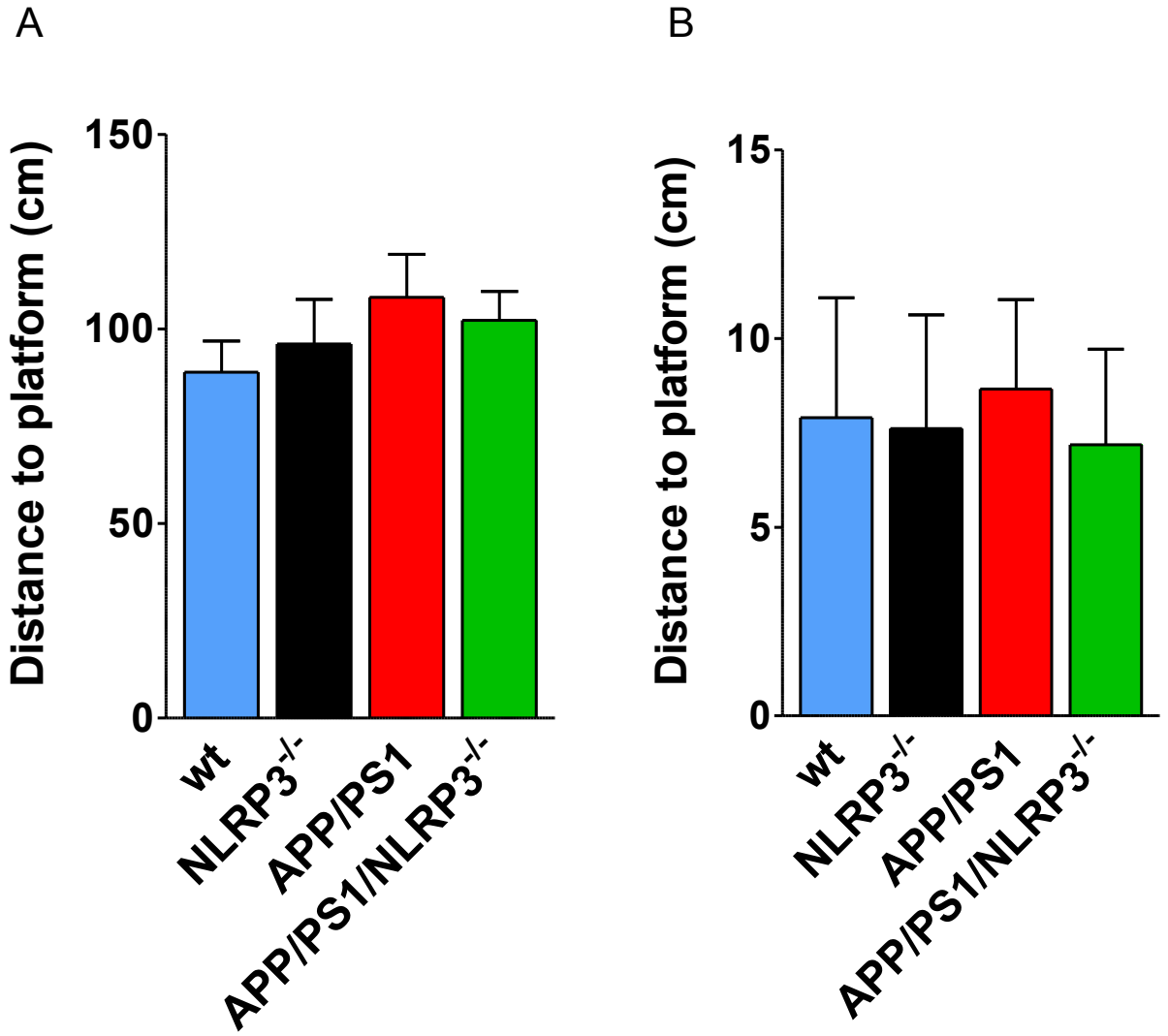

Suppl. Figure 5. Morris water maze - visual cue trial. At day 9, 4 h after spatial probe trials were conducted, a visual cue trial was performed and **(A)** distance to platform (cm) and **(B)** time to platform (sec) were recorded by the video tracking software (Ethovision 3.1, Noldus, The Netherlands) and subsequently analyzed. Statistical analysis did not reveal any significant differences between groups (mean of n=16 for wt, n=12 for NRLP3$^{-/-}$, n=14 for APP/PS1, and n=15 for APP/PS1/NLRP3$^{-/-}$ ±SEM; one-way ANOVA, Tukey´s post hoc test).

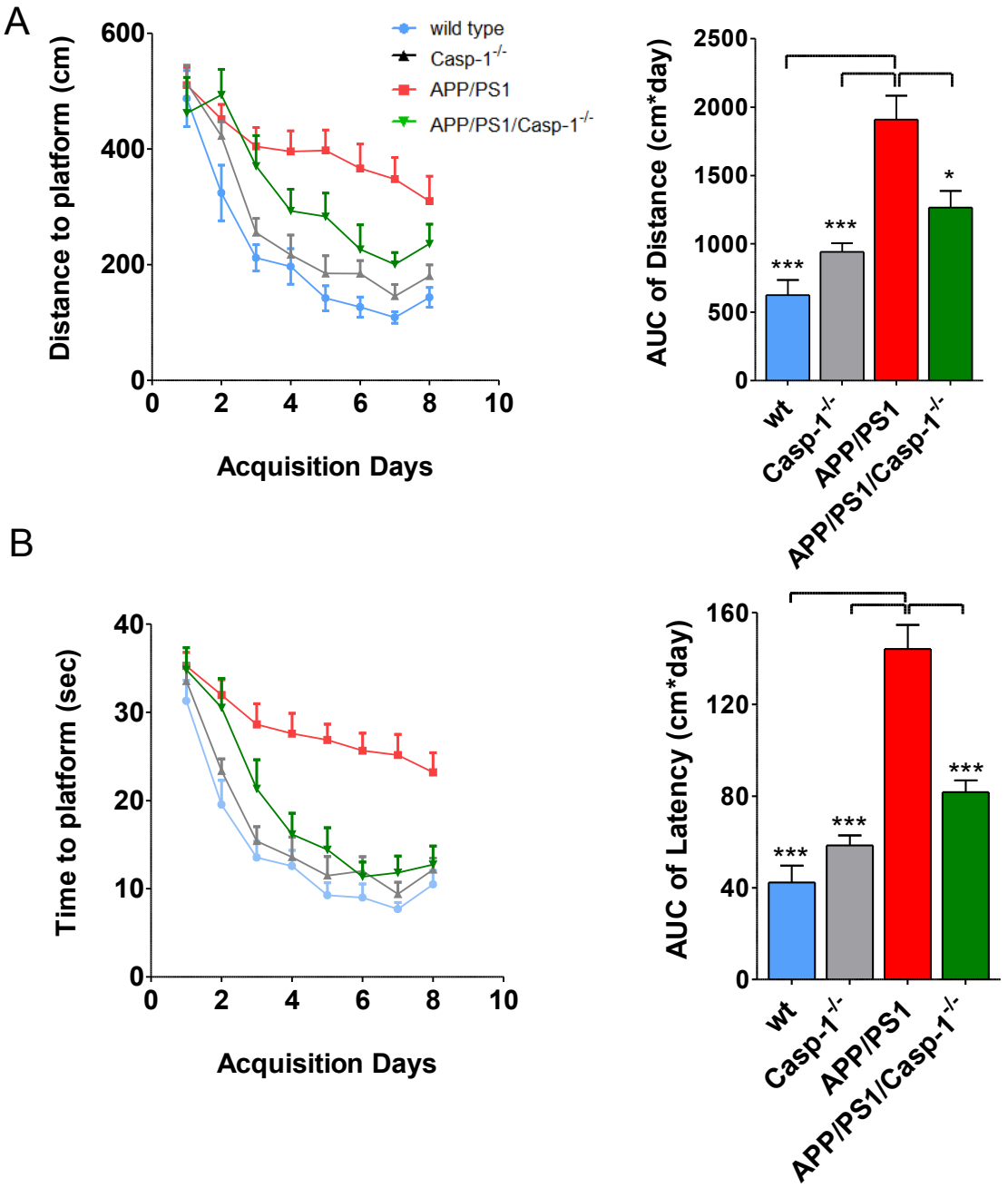

Suppl. Figure 6. Caspase-1 gene deficiency protects APP/PS1 transgenic mice from spatial memory deficits at 16 months of age. Spatial memory was assessed by Morris Water Maze testing: **(A)** Distance travelled to platform (Distance) and **(B)** time needed to reach the platform (latency) in wild-type (wt) caspase-1 deficient (Casp-1$^{-/-}$), APP/PS1 and APP/PS1/Casp-1$^{-/-}$ mice were recorded by the video tracking software (Ethovision 3.1, Noldus, The Netherlands) and subsequently analysed. Quantification was performed by integrating distance travelled and time needed to platform (area under the curve) (mean of n=13 for wt, n=17 for Casp-1$^{-/-}$, n=8 for APP/PS1, and n=13 for APP/PS1/Casp-1$^{-/-}$ ±SEM; one-way ANOVA, Tukey´s post hoc test, , * $p<0.05$, *** $p<0.001$).

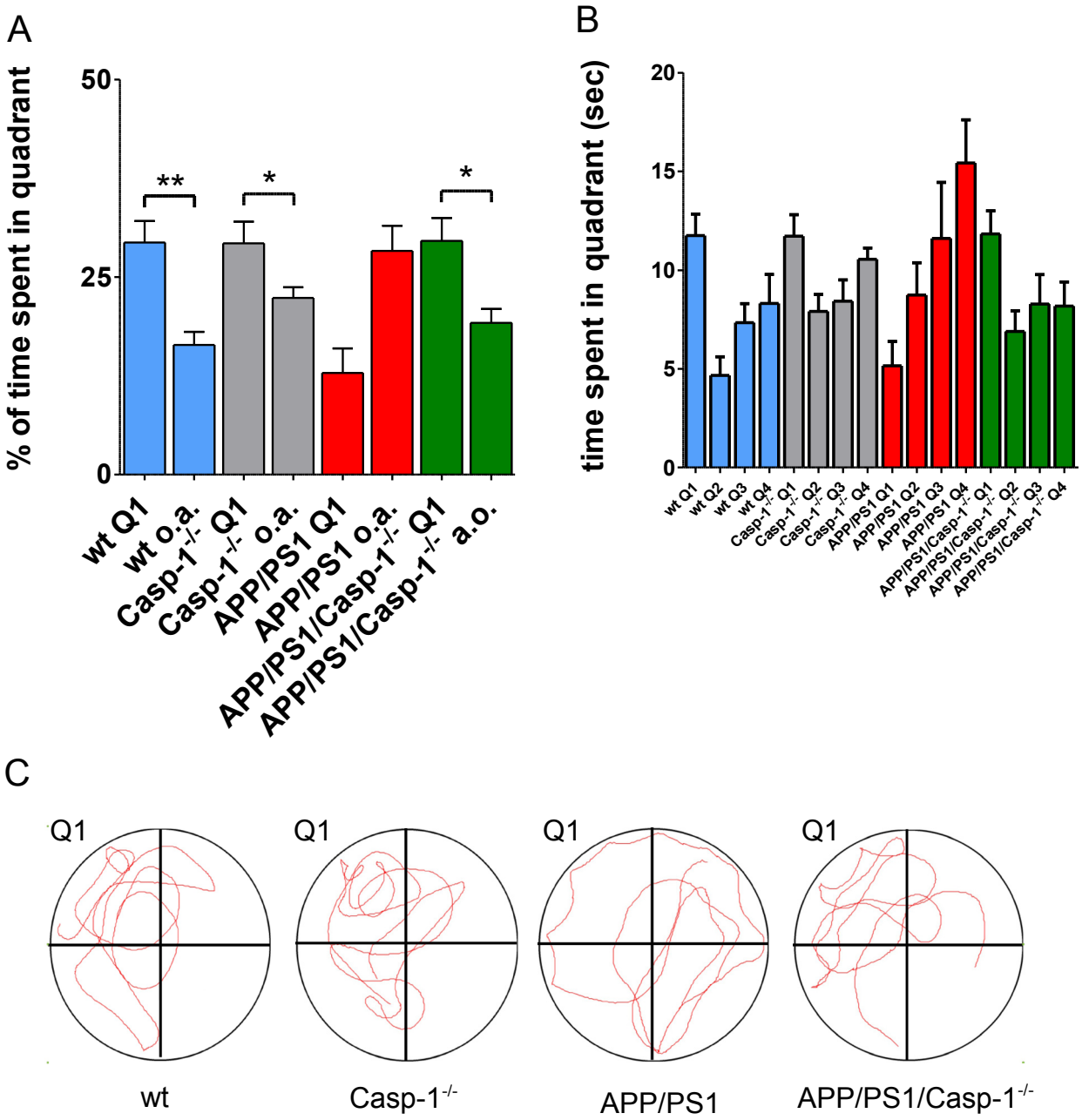

Suppl. Figure 7. Morris water maze - probe trial. At day 9, 24 h after the last training session, a spatial probe trial were conducted, where the platform was removed and the time animals spent in the quadrants was recorded. **(A)** Q1 represents the quadrant where the platform had been located from day 1-8. The values for the time spent in all other quadrants have been averaged (o.a.). Wt, Casp-$1^{-/-}$ and APP/PS1/Casp-$1^{-/-}$ showed a clear preference for the target quadrant Q1, whereas APP/PS1 mice failed to spent significantly more time in the target quadrant than in the other quadrants (mean of n=13 for wt, n=17 for Casp-$1^{-/-}$, n=8 for APP/PS1, and n=13 for APP/PS1/Casp-$1^{-/-}$ ±SEM; one-way ANOVA, Tukey´s post hoc test, * $p<0.05$, ** $p<0.01$). **(B)** Probe trial data from A, given as time spent in quadrant (sec) for each genotype and quadrant. **(C)** Representative runs of a single mouse are depicted. Q1 represents the quadrant where the platform had been located (day1-8).

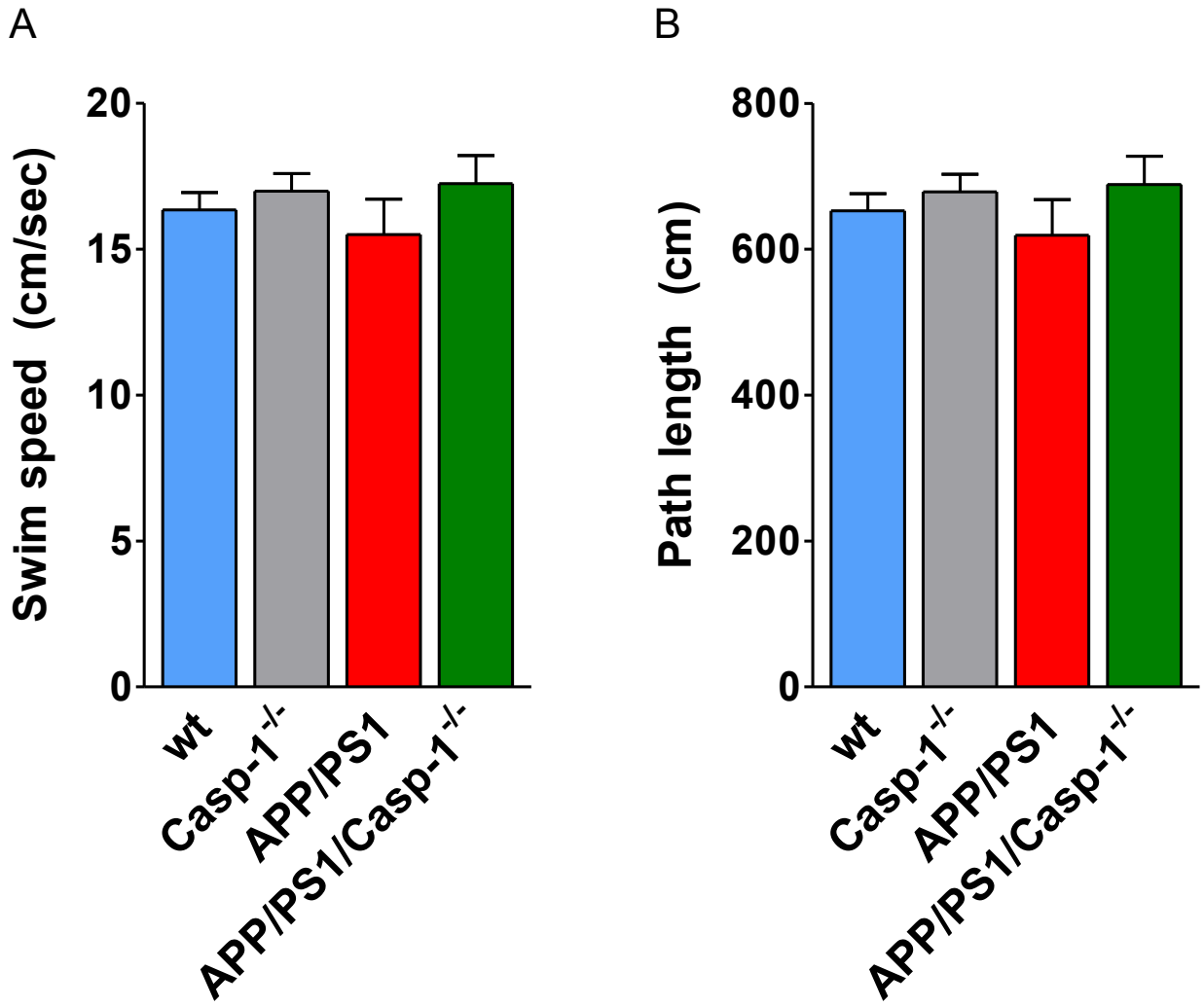

Suppl. Figure 8. Morris water maze - swim speed and path length. To exclude differences in motor performance between animal groups, **(A)** swim speed (cm/sec) and **(B)** path length (cm) during the Morris water maze test were recorded and analyzed by the video tracking software Ethovision 3.1 (Noldus, Wageningen, The Netherlands). Mean swim speed (v) was calculated by the equation v=distance/time and is given as cm/sec. Statistical analysis did not reveal any significant differences between groups (mean of n=13 for wt, n=17 for Casp-$1^{-/-}$, n=8 for APP/PS1, and n=13 for APP/PS1/Casp-$1^{-/-}$ ±SEM; one-way ANOVA, Tukey´s post hoc test).

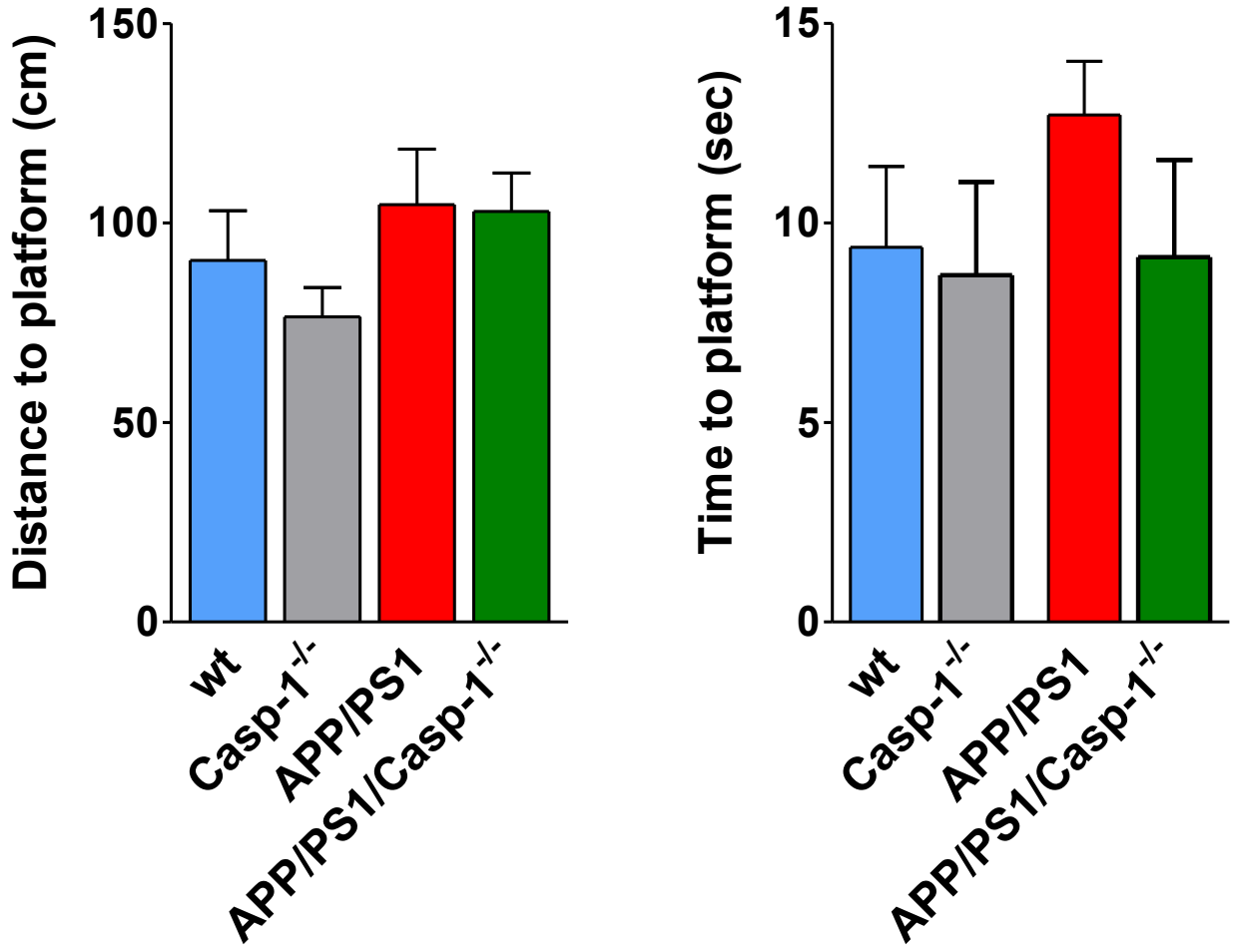

Suppl. Figure 9. Morris water maze - visual cue trial. At day 9, 4 h after spatial probe trials were conducted, a visual cue trial was performed and **(A)** distance to platform (cm) and **(B)** time to platform were recorded and analyzed by the video tracking software Ethovision 3.1 (Noldus, Wageningen, The Netherlands). Statistical analysis did not reveal any significant differences between groups (mean of n=13 for wt, n=17 for Casp-1$^{-/-}$, n=8 for APP/PS1, and n=13 for APP/PS1/Casp-1$^{-/-}$ ±SEM; one-way ANOVA, Tukey´s post hoc test).

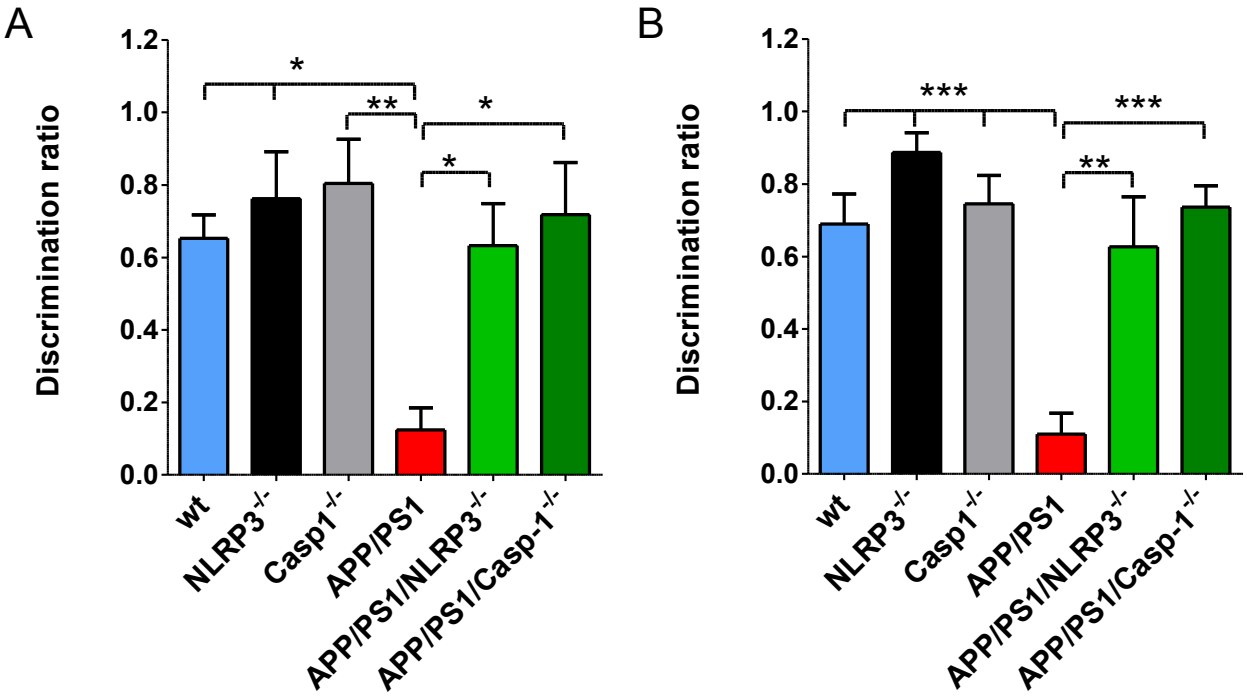

Suppl. Figure 10. Object recognition test. Object recognition was assessed in wild type (wt), NLRP3 deficient (NLRP3$^{-/-}$), caspase-1 deficient (Casp-1$^{-/-}$), APP/PS1, APP/PS1/NLRP3$^{-/-}$ and APP/PS1/Casp-1$^{-/-}$ mice at 16 months of age and tested object recognition at 10 min **(A)** and 24 h **(B)** after the sample-object exposure phase (mean of n=5 for wt, n=5 for NRLP3$^{-/-}$, n=10 for APP/PS1, n=7 for APP/PS1/NRLP3$^{-/-}$, n=13 for Casp-1$^{-/-}$, and n=9 APP/PS1/Casp-1$^{-/-}$ ± SEM; one-way ANOVA, Tukey´s post hoc test, * $p<0.05$,** $p<0.01$,*** $p<0.001$).

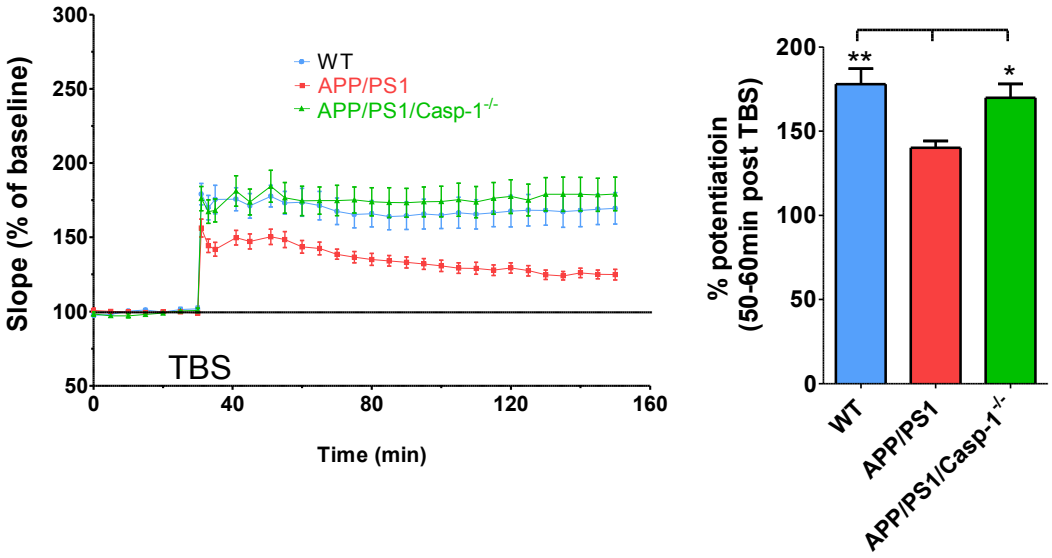

Suppl. Figure 11. Caspase-1 deficiency prevents suppression of long-term potentiation (LTP) in APP/PS1 mice. LTP was induced by theta-burst stimulation (TBS) 30 min after baseline recordings in hippocampal slices from WT, APP/PS1, and APP/PS1/Casp-1$^{-/-}$ mice. LTP quantification is given as % of potentiation 50-60 min post TBS (mean of WT, n=13, APP/PS1 n=17, APP/PS1/Casp-1$^{-/-}$ n=21 hippocampal slices measured ±SEM from n=6-9 animals per group; one-way ANOVA, Tukey´s post hoc test, * $p<0.05$,** $p<0.01$).

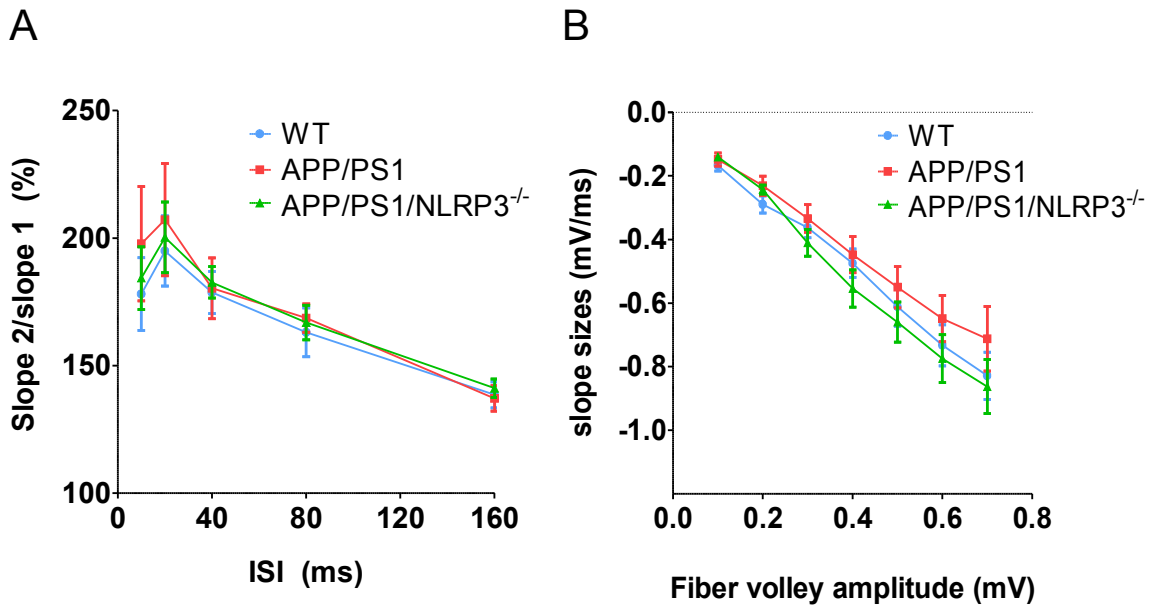

Suppl. Figure 12. NLRP3 gene deficiency does not affect paired-pulse facilitation in APP/PS1 transgenic mice. **(A)** Paired-pulse facilitation was unchanged between genotypes at all inter-stimulus intervals (ISI) tested. **(B)** Input-output curves revealed no alterations in basal synaptic transmission at defined fiber volley amplitudes (mean of WT, n=16, APP/PS1 n=23, APP/PS1/NLRP3-/- n=16 hippocampal slices measured ±SEM from n=6-9 animals per group; Student´s t-test). These data suggest that the observed effects on hippocampal LTP does not arise from changes in baseline synaptic transmission or short-term synaptic plasticity.

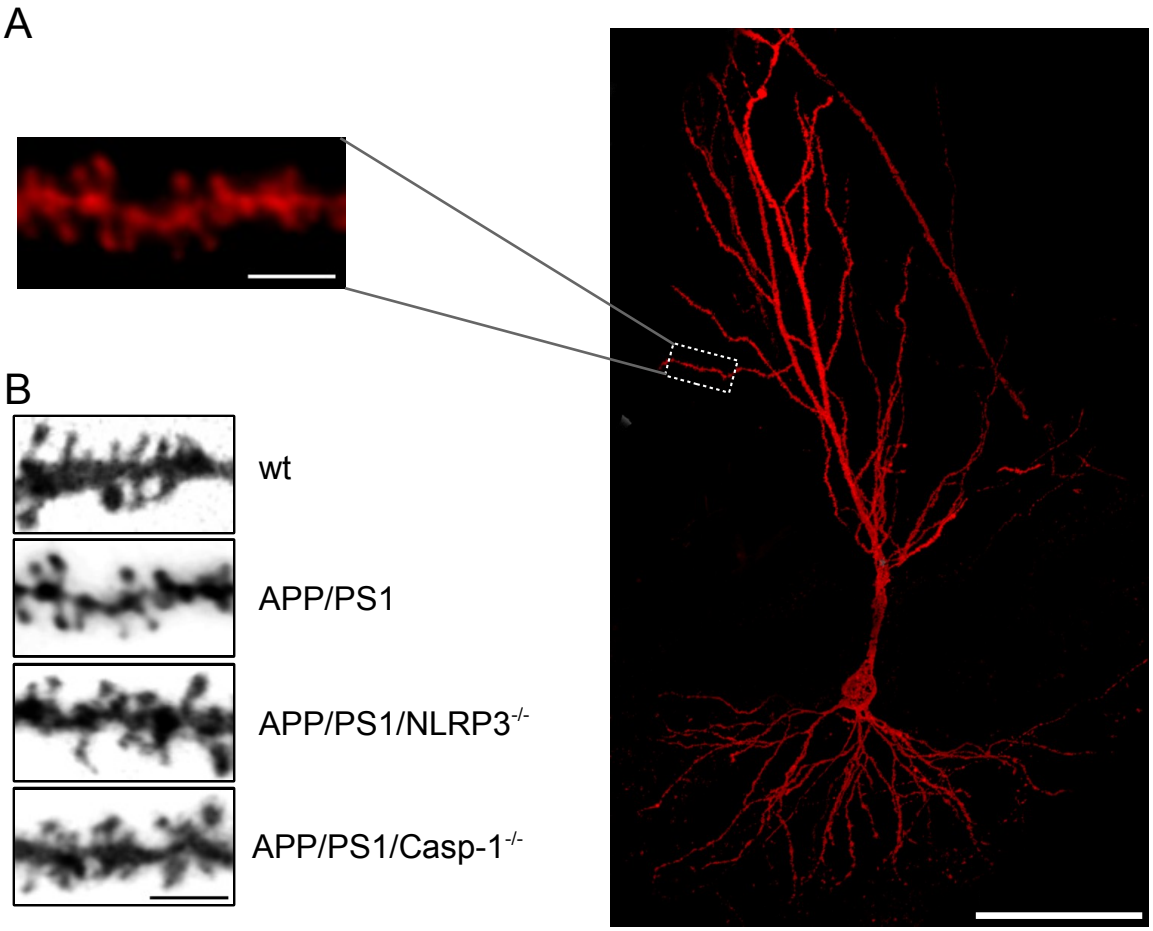

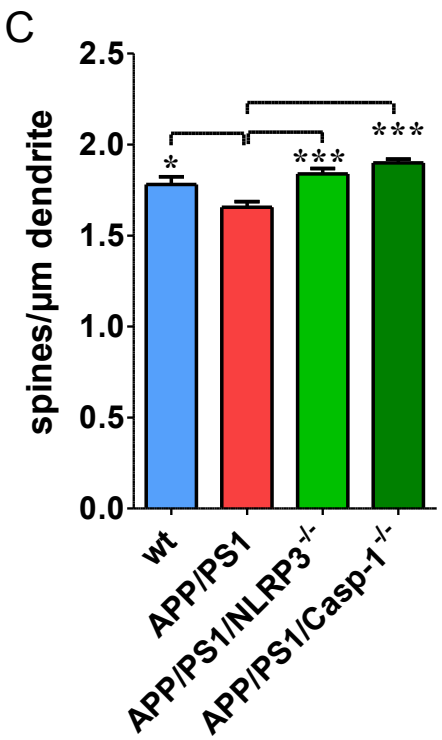

Suppl. Figure 13. Reduced spine density in APP/PS1 mice is rescued by NLRP3 or Casp-1 deficiency. (A) Representative image of a CA1 pyramidal neuron. The inserted square indicates the mid apical region used for spine density analysis (left panel: bar = 5 µm, right panel: bar = 100 µm). **(B)** Representative dendritic sections of the mid apical part of the different genotypes (bar = 5 µm) **(C)** Quantitative analysis of spine density from wild type (wt), APP/PS1, APP/PS1/NLRP3$^{-/-}$, and APP/PS1/Casp-1$^{-/-}$ neurons (mean of n=18 (for wt, n=31 for APP/PS1, n=25 APP/PS1/Casp-1$^{-/-}$, and n=11 for APP/PS1/NRLP3$^{-/-}$ ±SEM; one-way ANOVA, Tukey´s post hoc test, * $p<0.05$,*** $p<0.001$).

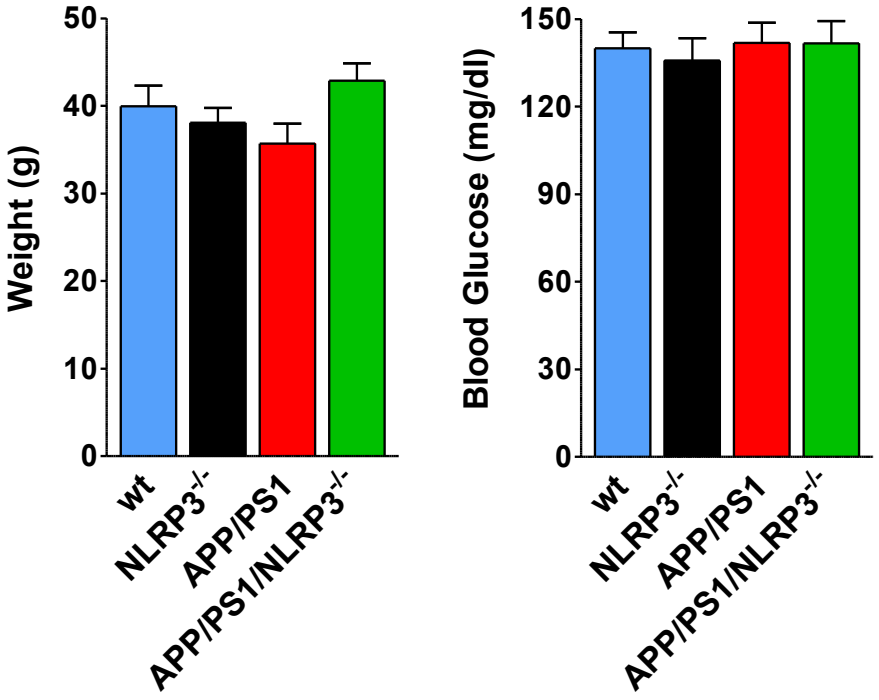

Suppl. Figure 14. NLRP3 gene deficient mice and controls do not differ in body weight or blood glucose levels. All animals studied were weighted and subjected to blood glucose analysis at 16 months of age before sacrifice. Statistical analysis did not reveal any significant differences between groups (mean of n=16 for wt, n=12 for NRLP3$^{-/-}$, n=14 for APP/PS1, and n=15 for APP/PS1/NLRP3$^{-/-}$ ±SEM, one-way ANOVA, Tukey's post hoc test).

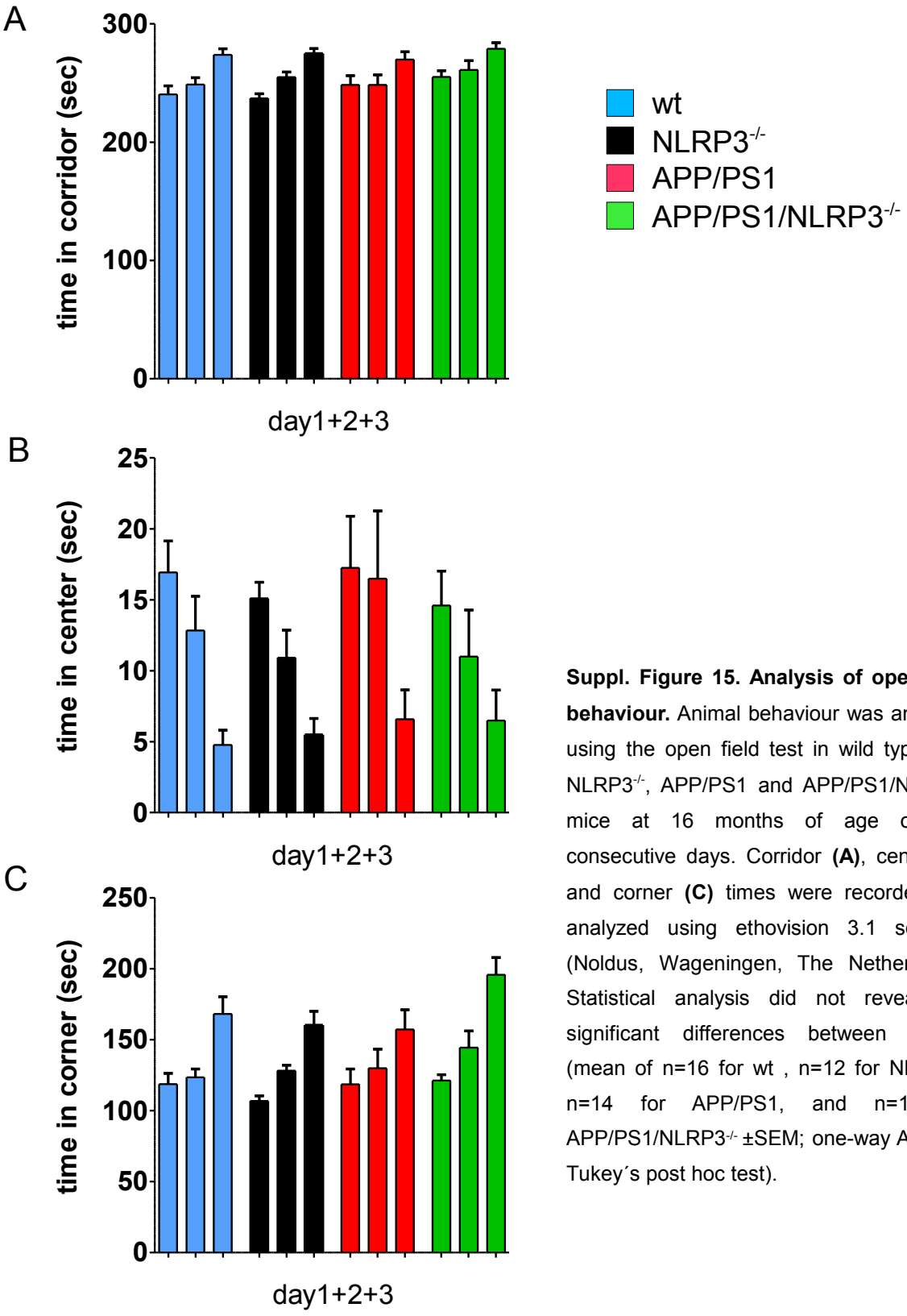

Suppl. Figure 15. Analysis of open field behaviour. Animal behaviour was analyzed using the open field test in wild type (wt), NLRP3$^{-/-}$, APP/PS1 and APP/PS1/NLRP3$^{-/-}$ mice at 16 months of age over 3 consecutive days. Corridor **(A)**, center **(B)** and corner **(C)** times were recorded and analyzed using ethovision 3.1 software (Noldus, Wageningen, The Netherlands). Statistical analysis did not reveal any significant differences between groups (mean of n=16 for wt , n=12 for NRLP3$^{-/-}$, n=14 for APP/PS1, and n=15 for APP/PS1/NLRP3$^{-/-}$ ±SEM; one-way ANOVA, Tukey´s post hoc test).

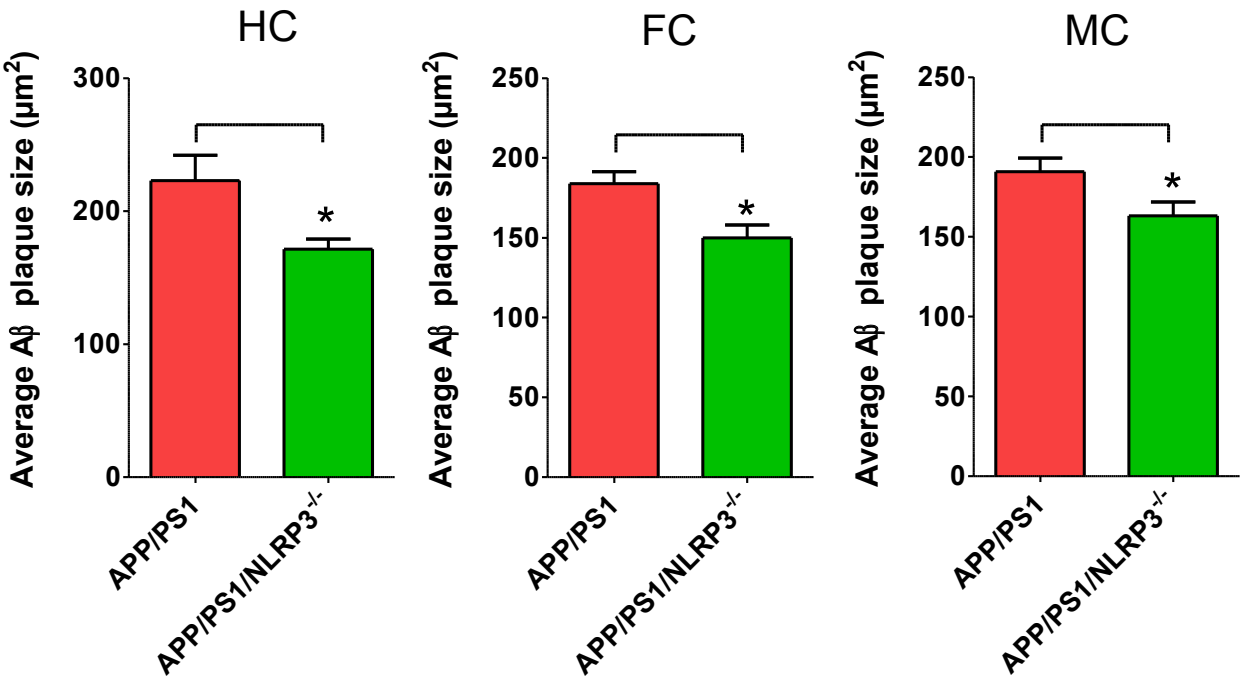

Suppl. Fig. 16. NLRP3 gene deficiency leads to decreased Aβ deposition. Aβ plaque deposition of APP/PS1 and APP/PS1/NLRP3$^{-/-}$ mice was quantified in the hippocampus (HC), frontal cortex (FC) and motor cortex (MC) using thioflavin S histochemistry. Quantification of the average Aβ plaque size was performed by analyzing 5 consecutive sections with defined distance per animal (mean of n=7-8 ±SEM; Student´s t-test, * $p<0.05$).

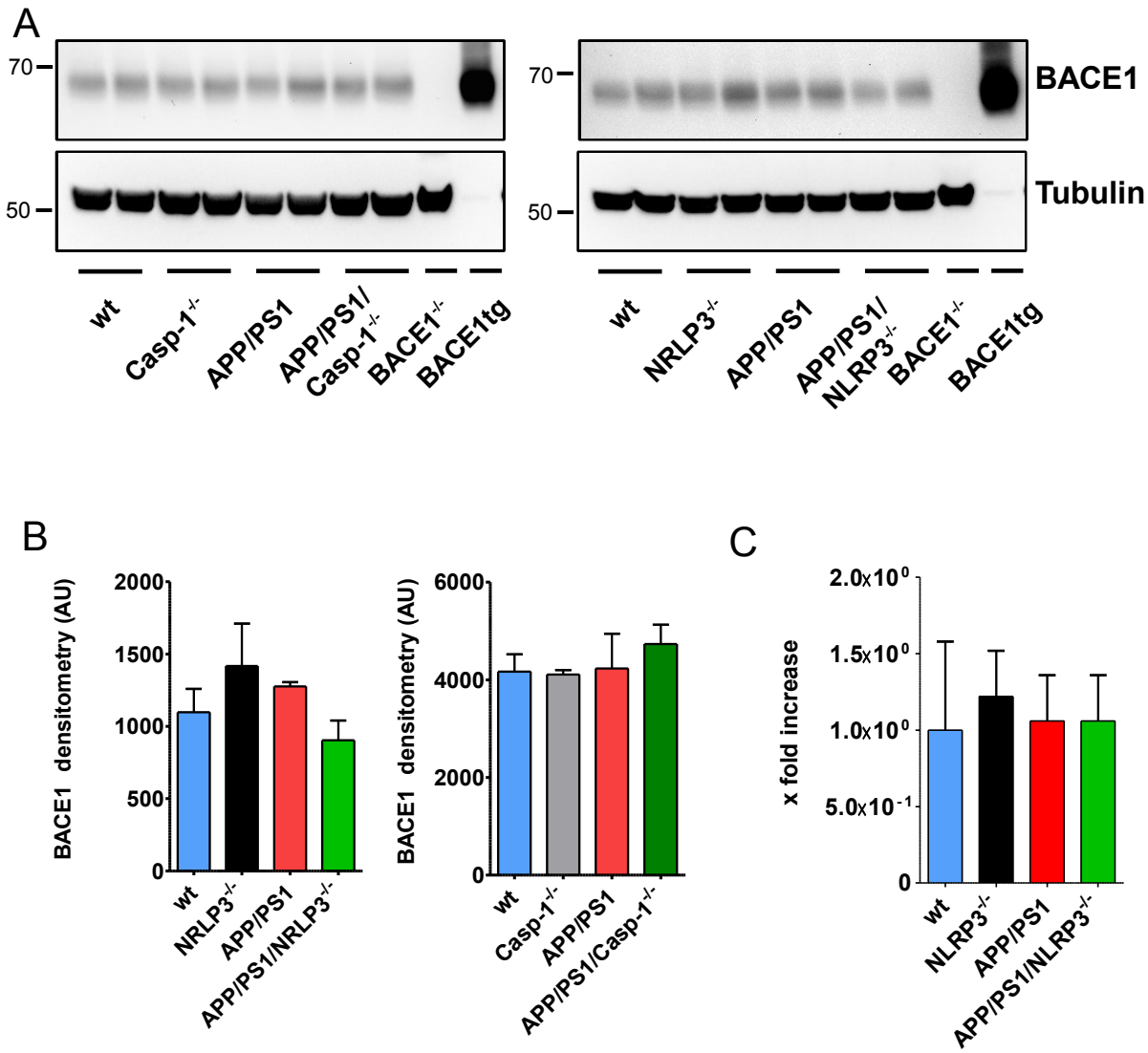

Suppl. Figure 17. NLRP3 gene deficiency does not affect β-secretase-1 mRNA and protein levels. As inflammatory signals can modulate APP processing and increase Aβ secretion through increase of β-secretase-1 (BACE1), wt, Casp-1$^{-/-}$, NLRP3$^{-/-}$, APP/PS1, APP/PS1/Casp-1$^{-/-}$ and APP/PS1/NLRP3$^{-/-}$ mice were tested for cerebral BACE1 protein levels. **(A)** Western blot detection of murine brain lysates of each genotype for BACE1. Brain lysates from BACE1 deficient mice (BACE1$^{-/-}$, gift from Dr. B. De Strooper, UKL Leuven, Leuven, Belgium) served as negative controls. Brain lysates derived from BACE1 overexpressing mice (BACE1 tg, gift from Dr. H. Jacobsen, Roche, Basel, Switzerland) served as positive controls, but 10 times less protein was loaded due to the high expression of transgenic BACE1. β-actin served as loading control. **(B)** Quantification of BACE1 protein (mean of n=2 ± SEM; one-way ANOVA, Tukey's post hoc test) or **(C)** mRNA levels did not show any significant differences, suggesting that inflammatory modulation of BACE1 is not involved in the observed effects of NLRP3 on cerebral Aβ load (mean of n=5 ± SEM; one-way ANOVA, Tukey's post hoc test).

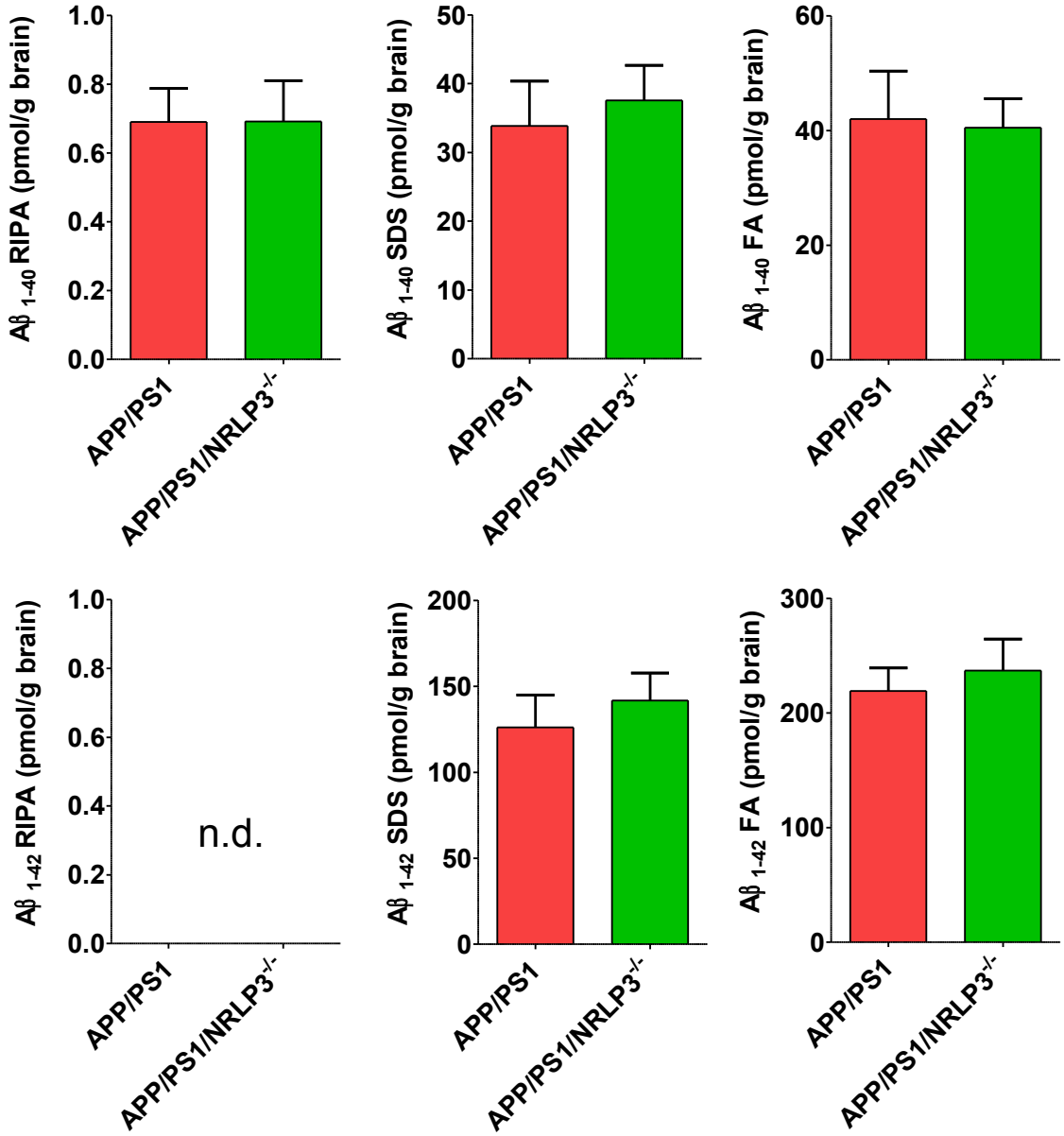

Suppl. Figure 18. NLRP3 gene deficiency does not affect cerebral Aβ load at 4 months of age in APP/PS1 mice. ELISA quantification of SDS and RIPA soluble fractions for Aβ1-40 and 1-42 from 4 months old APP/PS1 and APP/PS1/NLRP3$^{-/-}$ mice (mean of n=4 ± SEM; Student's t-test; n.d.= not detectable).

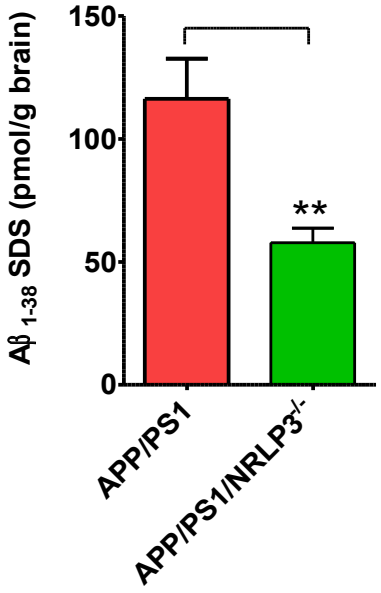

Suppl. Figure 19. NLRP3 gene deficiency decreases $A\beta_{1-38}$. ELISA quantification of Aβ1-38 was performed in SDS fractions of 16 months old APP/PS1 and APP/PS1/NLRP3$^{-/-}$ mice. Aβ1-38 was undetectable in the RIPA fraction (not shown), however, analysis of the SDS fraction showed that NLRP3 gene deficiency almost halved Aβ1-38. (mean of n=5 ± SEM; Student's t-test, ** $p<0.01$).

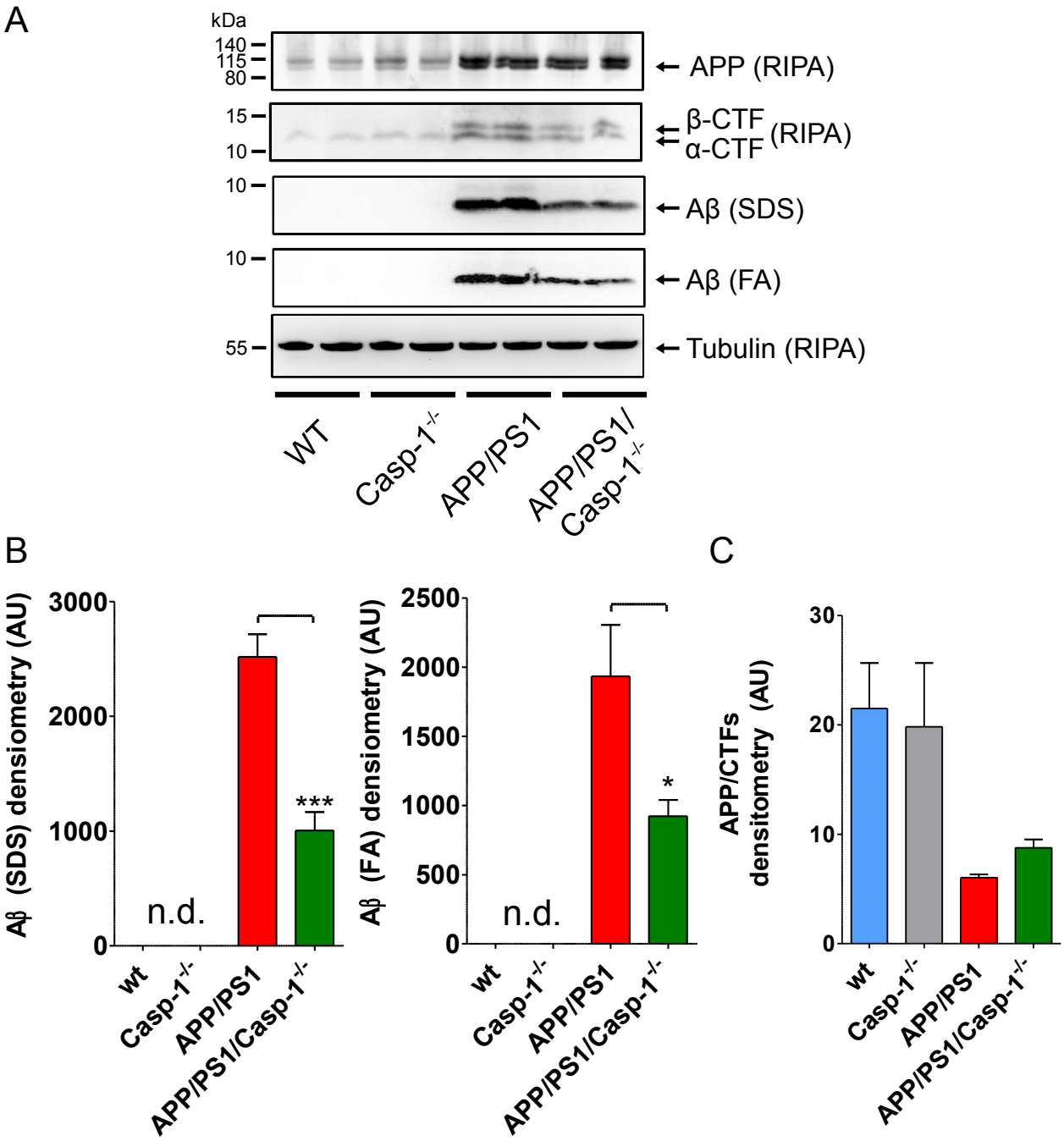

Suppl. Figure 20. APP/PS1/Casp-1 gene deficiency reveals reduced cerebral Aβ load at 16 months of age. (A) Western blot analysis of RIPA, SDS, and FA brain extracts of 16 months old wild type (WT), Casp-$1^{-/-}$, APP/PS1, and APP/PS1/Casp-$1^{-/-}$ mice using antibodies CT15 for APP and CTF and 6E10 for Aβ. Tubulin served as a loading control. **(B)** Densitometrical quantification of SDS and FA-soluble Aβ. **(C)** Ratio of APP to CTFs reveal no differences between APP/PS1 and APP/PS1/Casp-$1^{-/-}$ mice (mean of n=4 ± SEM; Student´s t-test, * $p<0.05$, n.d. = not detectable).

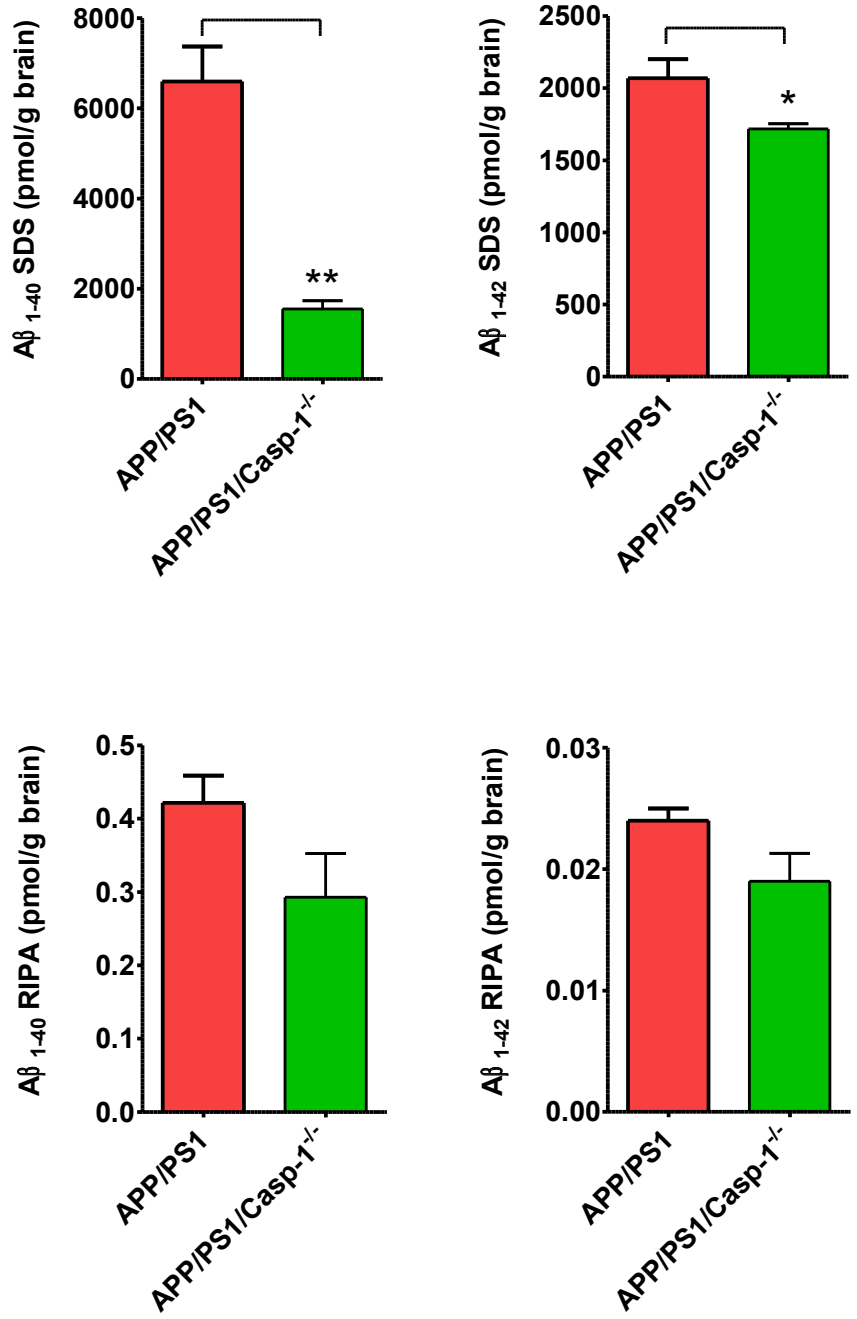

Suppl. Figure 21. APP/PS1/Casp-1 gene deficiency reveal reduced cerebral Aβ load at 16 months of age. ELISA quantification of SDS and RIPA soluble fractions for Aβ1-40 and 1-42 from 16 months old APP/PS1 and APP/PS1/Casp-1$^{-/-}$ mice (mean of n=4 ± SEM; Student's t-test, * p<0.05, ** p<0.01).

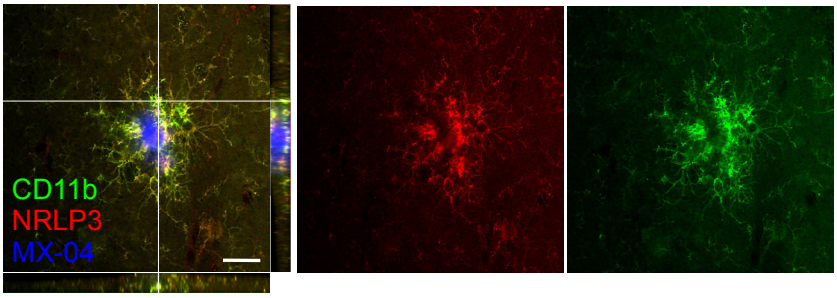

Suppl. Figure 22. Immunohistochemical detection of NLRP3 in Aβ plaque-associated microglia. In order to verify microglial NLRP3 expression in APP/PS1 mice, we immunostained brain sections from APP/PS1 at 16 months for NLRP3 and CD11b. NLRP3 expression was colocalized with CD11b in microglia surrounding Aβ deposits, visualized by methoxy-X04 (bar = 20 μm).

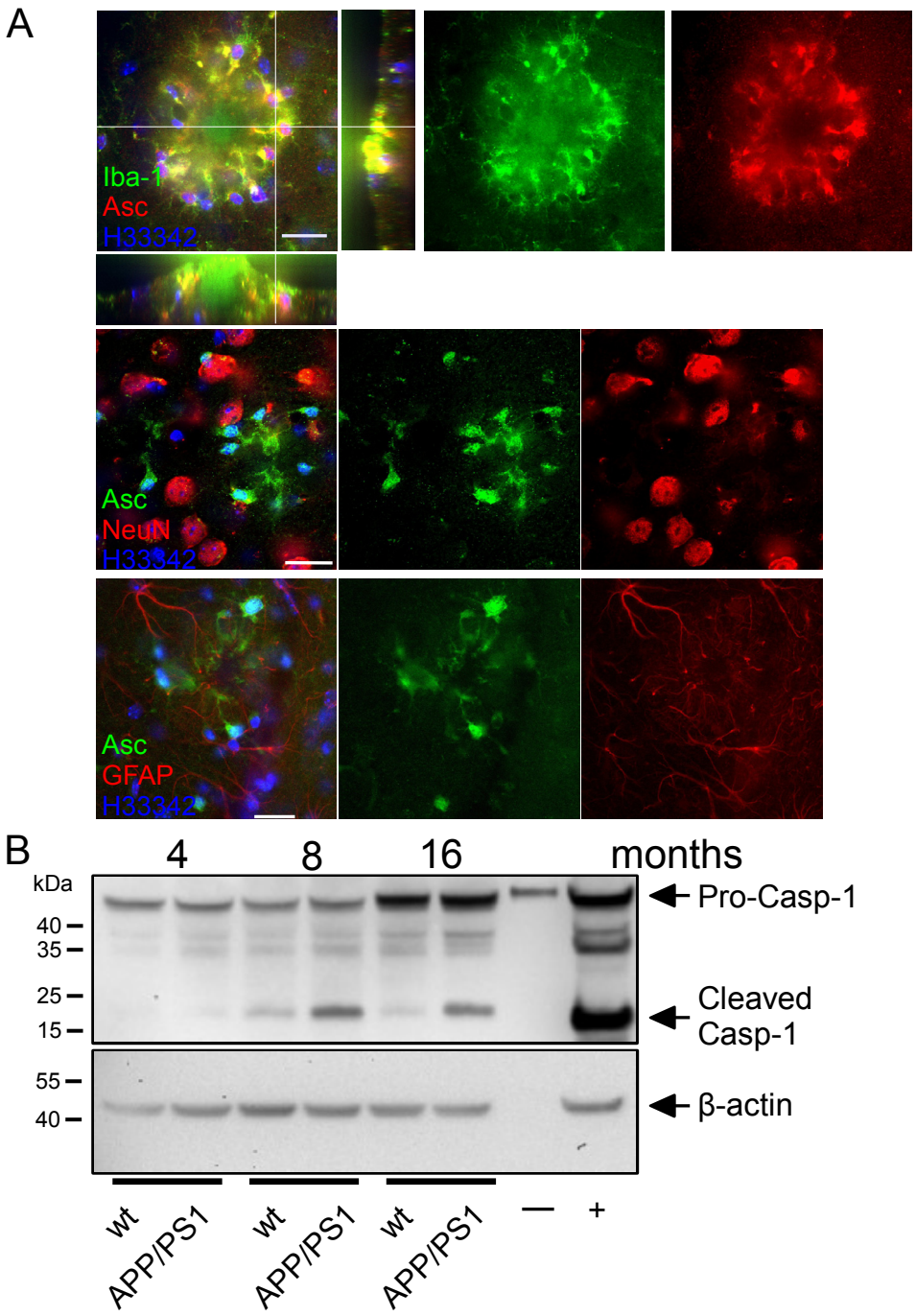

Suppl. Figure 23. Characterization of inflammasome activation in APP/PS1 mice. (A) Co-immunostaining for apoptosis-associated speck-like protein containing a caspase recruitment domain (Asc) and the microglia marker Iba-1 detected Asc exclusively in Iba-1-positive microglia and was neither colocalized to the neuronal marker NeuN nor the astroglial marker glial fibrillary acidic protein (GFAP). H33342 served as nuclear stain (bar = 20 µm). **(B)** Detection of cleaved caspase-1 as marker of NLRP3 inflammasome activation in cerebral lysates from wild-type and APP/PS1 mice at 4, 8 and 16 months of age. Actin served as loading control. Supernatant from wildtype, immortalized murine macrophages treated with 200 ng/ml bacterial lipopolysaccharide for 3 h and 10 µM nigericin for 1 h served as positive control.

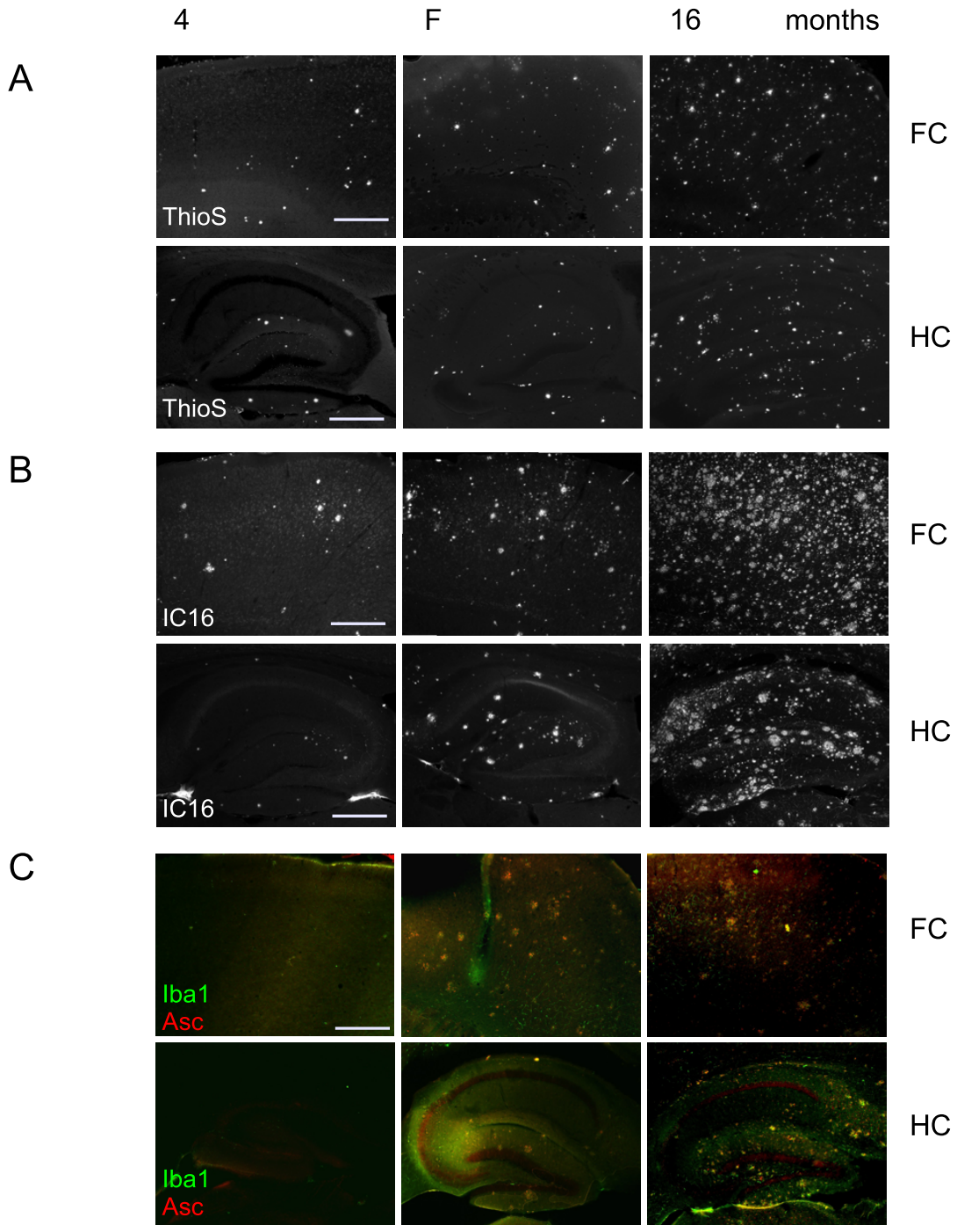

Suppl. Figure 24. Characterization of inflammasome activation in APP/PS1 mice in relation to A@ deposition. (A) Thioflavin S (ThioS) histochemistry and **(B)** Aβ immunohistochemistry using antibody IC16 were used to visualize the age-dependent deposition of Aβ in the frontal cortex (FC) and hippocampus (HC) of APP/PS1 mice at 4, 8 and 16 months of age. **(C)** Parallel brain sections from the same mice were used to analyze the age-dependent activation of the inflammasome by immunostaining for the apoptosis-associated speck-like protein containing a caspase recruitment domain (Asc) and the microglia marker Iba-1 (bar = 500 µm).

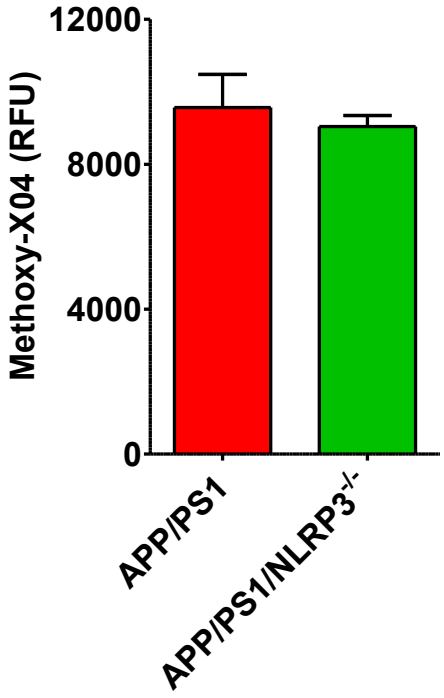

Suppl. Figure 25. Cerebral Methoxy-X04 levels are not affected by NLRP3 deficiency. To exclude that differences of microglia phagocytosis between APP/PS1 and APP/PS1/NRLP3$^{-/-}$ mice are based on varying cerebral levels of methoxy-X04, mice were peripherally injected with methoxy-X04 and brain homogenates were determined for methoxy-X04 fluorescence 3 h later. Statistical analysis did not reveal any significant differences between groups (mean of n=7 for APP/PS1 and n=6 for APP/PS1/NRLP3$^{-/-}$ ± SEM; ANOVA and Tukey´s post hoc test).

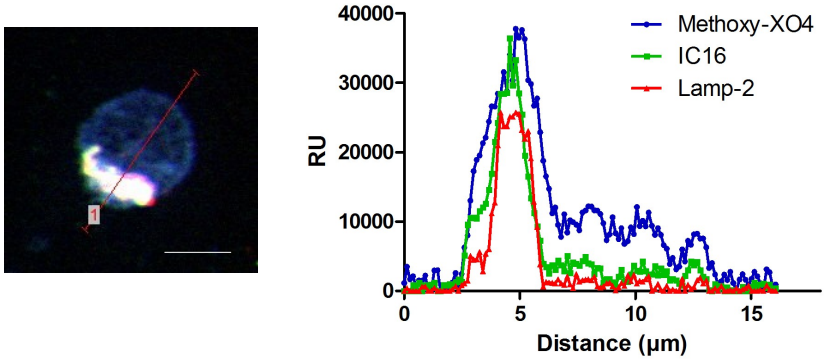

Suppl. Figure 26. Fluorescence intensity profile of a microglia cell shown in Figure 3D. (bar = 5 µm).

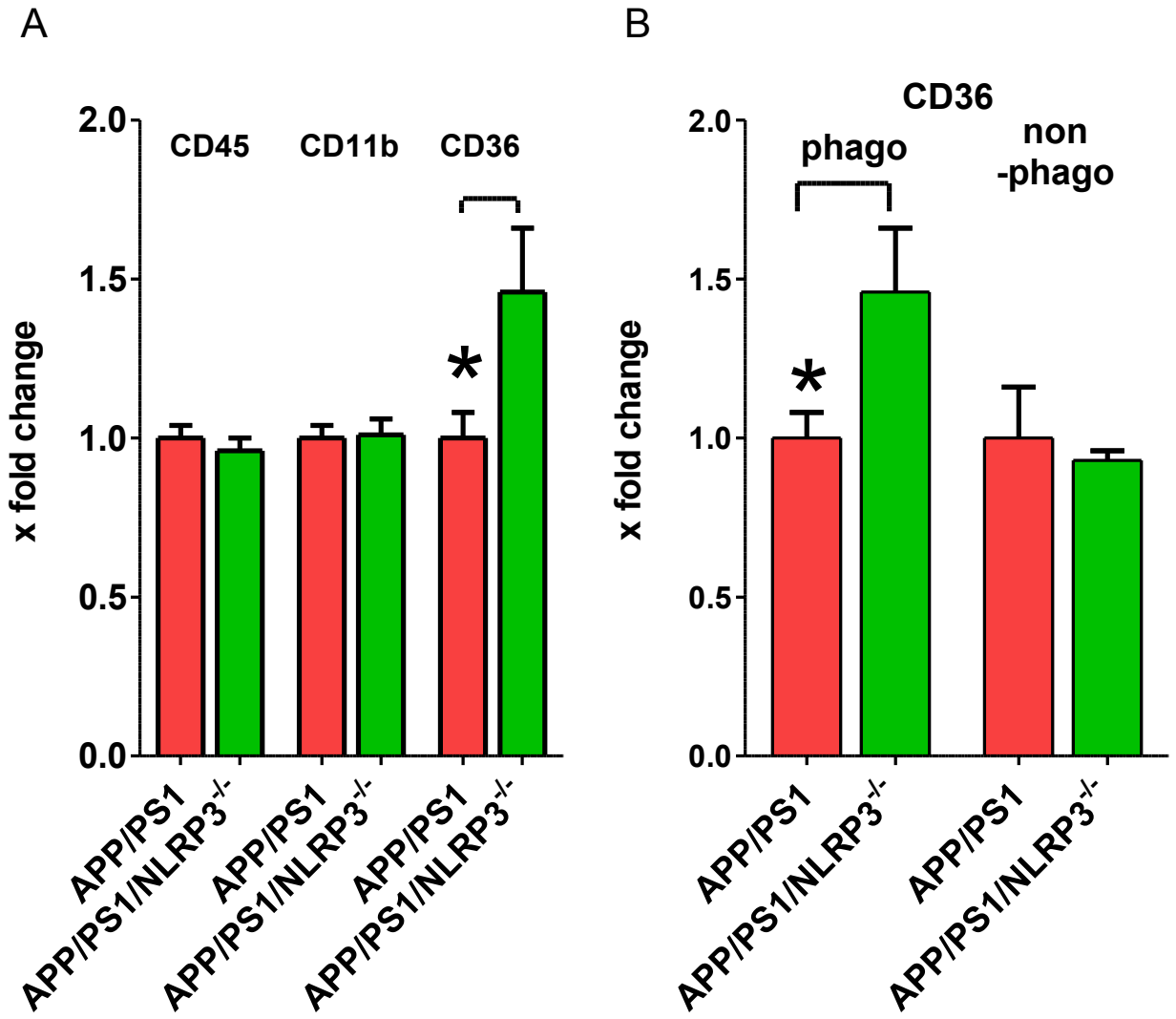

Suppl. Figure 27. Increased expression of CD36 on phagocytic microglia of NLRP3 gene deficient APP/PS1 mice. Phagocytosis of deposited Aβ was analyzed 3h after peritoneal application of the amyloid dye methoxy-X04 by flow cytometry of isolated adult microglia. (**A**) Cells were analyzed for the expression of the CD45, CD11b, CD36 isolated from APP/PS1 and APP/PS1/NLRP3$^{-/-}$ mice at 8 months of age (mean of n=4-5 ± SEM; Student's t-test, * $p<0.05$). (**B**) Expression of CD36 was compared between CD11b^{+}, methoxy-X04^{-} (non-phagocytic microglia; non-phago) and CD11b^{+}, methoxy-X04^{+} cells (phagocytic microglia; phago) from APP/PS1 and APP/PS1/NLRP3$^{-/-}$ mice at 8 months of age revealing increased expression of CD36 on phagocytic microglia (mean of n=4-5 ± SEM; Student's t-test, * $p<0.05$).

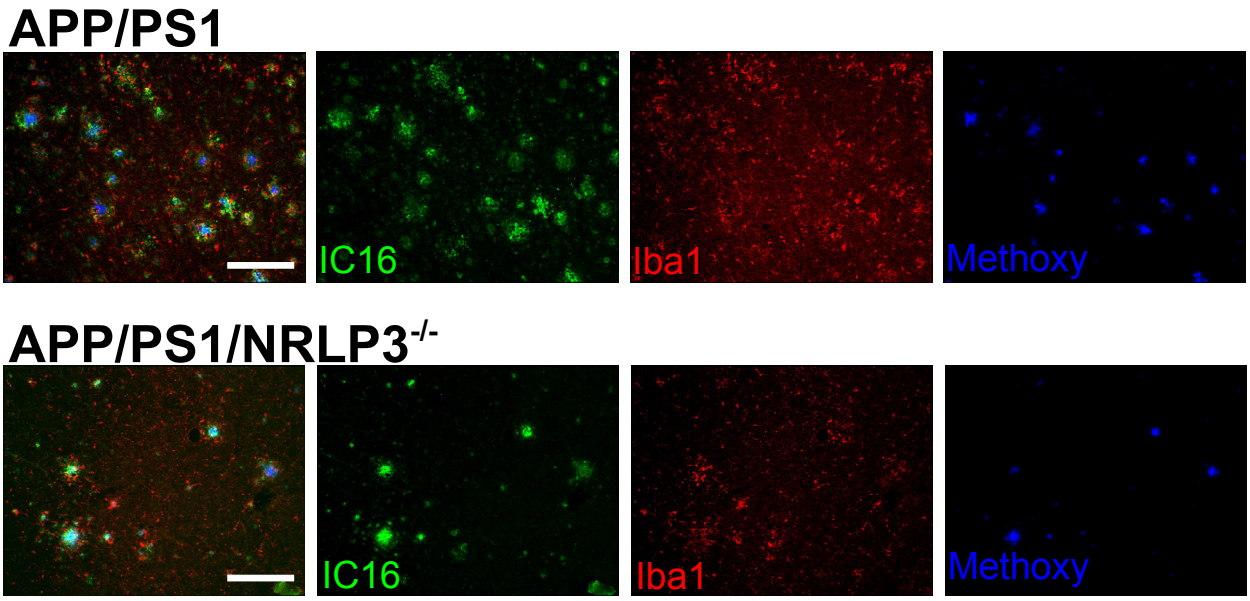

Suppl. Figure 28. Immunohistochemistry of Aβ deposition and microglial activation in APP/PS1 and APP/PS1/NLRP3$^{-/-}$ mice. Serial sagittal sections of methoxy-XO4-treated, 16 months old APP/PS1 and APP/PS1/NLRP3$^{-/-}$ mice were immunostained for Aβ deposition by antibody IC16. Microglial activation was assessed by staining for Iba-1. Representative images of the neocortex of APP/PS1 and APP/PS1/NLRP3$^{-/-}$ mice are shown (bar= 200 μm).

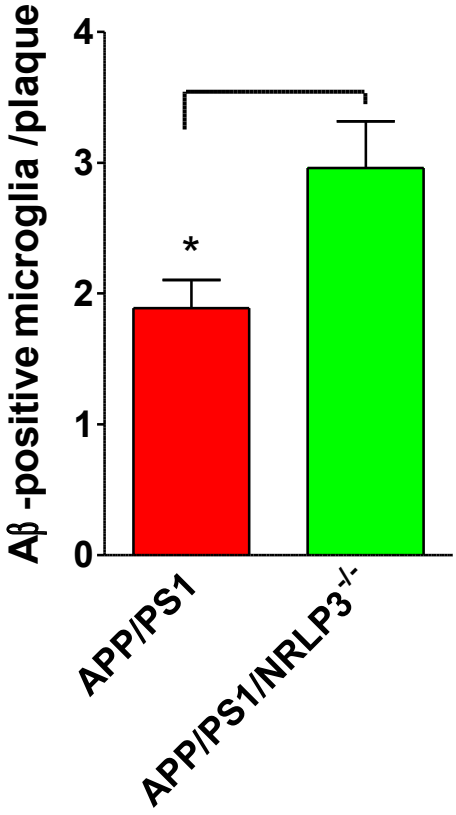

Suppl. Figure 29. Immunohistochemical detection of Aβ within microglia. The number of Iba-1-positive microglia conatining IC16-positive material was assessed in the frontal cortex by laser scanning microscopy (mean of n=24± SEM from 3 mice per group; Student's t-test, * $p<0.05$).

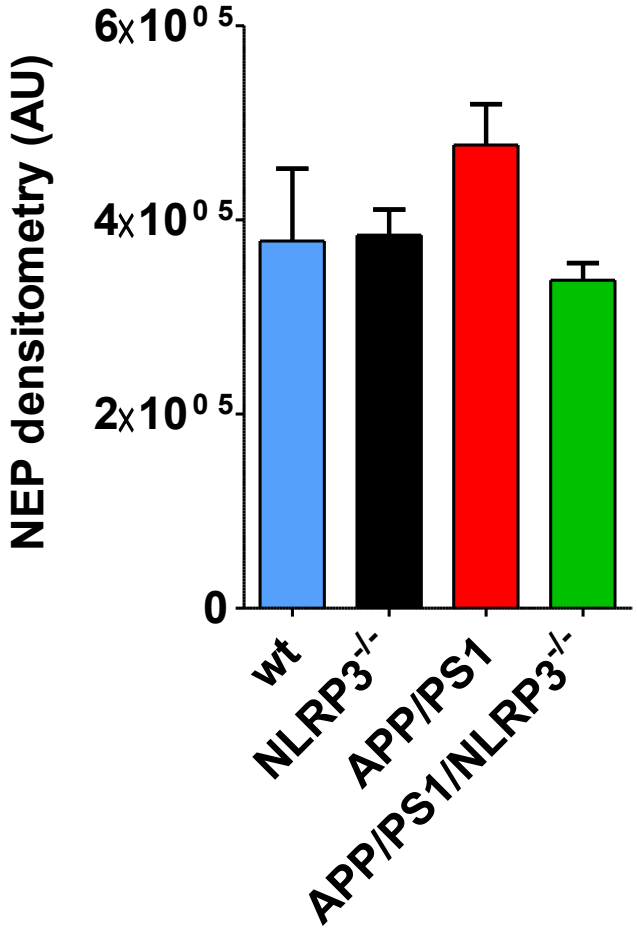

Suppl. Figure 30. Neprilysin protein levels remain unaffected by NLRP3. At 16 months of age, wildtype (wt), NLRP3$^{-/-}$, APP/PS1 and APP/PS1/NLRP3$^{-/-}$ mice were tested for neprilysin (NEP) protein levels by Western blot analysis. Similar to IDE, NEP represents a key enzyme for cerebral Aβ degradation. Data are given as mean ± SEM. Statistical analysis did not reveal any significant differences between groups (mean of n=5 ± SEM; one-way ANOVA, Tukey's post hoc test).

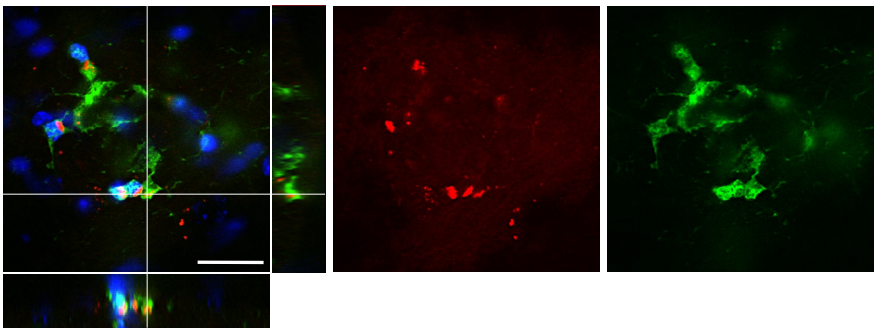

Suppl. Figure 31. Immunohistochemical detection of found in inflammatory zone-1 (FIZZ1) in microglia. In order to verify the microglial nature of FIZZ-1 expression in APP/PS1 mice, we analyzed brain sections from APP/PS1/CX3CR1-EGFP$^{+/-}$ mice at 16 months of age. In this model, microglia cells express EGFP under the control of the CX3CR1 promoter, restricting its expression to microglia/macrophages. Immunostaining for FIZZ1 was exclusively found in EGFP-positive microglia. H33342 was used as a nuclear stain (bar = 20 µm).